Supplementary Information for

Dissecting single-molecule signal transduction by carbon nanotube circuits with protein engineering

Yongki Choi,[1,*] Tivoli J. Olsen,[2,*] Patrick C. Sims,[1] Issa S. Moody,[3] Brad L. Corso,[1] Mytrang N. Dang,[2] Gregory A. Weiss[2,3] and Philip G. Collins[1]

[1]*Departments of Physics and Astronomy,* [2]*Chemistry, and* [3]*Molecular Biology and Biochemistry, University of California, Irvine, CA 92697, United States*

[*]*These authors contributed equally to this work*

Correspondence and requests for materials should be addressed to G.A.W. (email: gweiss@uci.edu) or P.G.C.(email: collinsp@uci.edu)

Contents of the Supplementary Information

1. Materials

Reagents purchased commercially include antibiotics (Fisher Scientific), cation exchange resin (Bio-Rad Laboratories), cell lines (Stratagene), DNA purification kits (Invitrogen, Qiagen or Zymo Research), deoxyribonucleotides (Promega Corporation), enzymes (New England Biolabs or Fermentas), oligonucleotides (IDT), and 96-well plates (Nunc). Other chemicals were purchased commercially from Acros Organics, EMD, Fisher Scientific, or Sigma Aldrich. Unless otherwise indicated below, reagents were used as received.

2. Lysozyme Synthesis and Purification

2A. Mutagenesis of T4 lysozyme

A pET28 bacterial expression vector containing the gene encoding the S90C lysozyme variant was previously described[1, 2]. Additional variants of lysozyme were engineered using QuikChange® site-directed mutagenesis (Stratagene) with the following oligonucleotides.

Oligonucleotides (mutations denoted in bold):

S90C/K83A_FWD	5'-GTTCGCGGAATTCTGAGAAATGCT**GC**ATTAA AACCGGTTTATGATTGTCTTGA-3'
S90C/K83A_REV	5'-CGCATCAAGACAATCATAAACCGGTTTTAA**T** **G**CAGCATTTCTCAGAATTCCGCG-3'
S90C/K83E_FWD	5'-GTTCGCGGAATTCTGAGAAATGCT**G**AATTA AAACCGGTTTATGATTGTCTTGA-3'
S90C/K83E_REV	5'-CGCATCAAGACAATCATAAACCGGTTTTAATT**C** AGCATTTCTCAGAATTCCGCG-3'

S90C/R119A_FWD	5'-GGATTTACTAACTCTTTA**GC**TATGCTTCAACA AAAACGCTGG-3'
S90C/R119A_REV	5'-GCGTTTTTGTTGAAGCATA**GC**TAAAGAGTTAG TAAATCCTGC-3'
S90C/R119E_FWD	5'-GGATTTACTAACTCTTTA**GAA**ATGCTTCAACA AAAACGCTGG-3'
S90C/R119E_REV	5'-GCGTTTTTGTTGAAGCAT**TTC**TAAAGAGTTAG TAAATCCTGC-3'

2B. Expression of T4 lysozyme variants

Plasmids containing genes encoding for variants of lysozyme were transformed by heat shock into $CaCl_2$ competent BL21(DE3) *E. coli*. Single colonies were selected for overnight incubation in 25 mL of LB supplemented with kanamycin (40 μg/ml) at 37 °C. The overnight culture (10 mL) was added to 1 L of fresh LB supplemented with kanamycin (40 μg/ml), and grown for several hours at 37 °C. When the cells reached late log phase (OD_{600} = 0.8), protein expression was induced by the addition of 1 mM IPTG. After induction, lysozyme variants were overexpressed for 5 h at 30 °C. At the time of induction, 1 mM phenylmethylsulfonyl fluoride (PMSF) was added to the culture containing the K83A/R119A/S90C variant to slow proteolysis.

2C. Purification of T4 lysozyme variants

A typical purification scheme included the following steps. After overexpression, cells were harvested by centrifugation (1000 g, 20 min, 4 °C) and resuspended in lysis buffer (20 mM Tris, 10 mM NaCl, pH 7.5). Cells were lysed by sonication and centrifuged (20,000 g, 50 min, 4 °C) to remove cell debris. After centrifugation, the crude cell lysate was filtered (0.45 μm pore size) prior to FPLC (Bio-Rad Biologic DuoFlow FPLC) using cation exchange chromatography and eluted with a gradient of 1 M NaCl. Fractions containing the protein were concentrated before filtration through a 0.45 μm filter. Further purification applied size exclusion chromatography in PBS (140 mM NaCl, 2.7 mM KCl, 8.1 mM Na_2HPO_4, 1.5 mM KH_2PO_4, pH 7.2). The purity of each T4 lysozyme variant was assessed by SDS-PAGE (Figure S1).

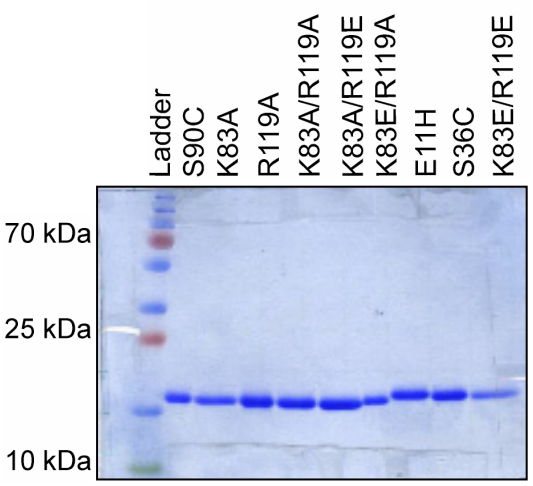

Figure S1. A 15% SDS-PAGE of lysozyme variants after cation exchange and size exclusion chromatography. Each T4 lysozyme variant was purified to >95% homogeneity and migrated at the expected mass of ~18 kDa.

2D. Circular dichroism of T4 lysozyme variants

The circular dichroism spectra of the T4 lysozyme variants (15 μM) were acquired using a spectropolarimeter (JASCO model J-810) at 22 °C with the following parameters: 1.0 nm bandwith, 0.1 cm path length, 2.0 s response time, and 10 nm/min scanning speed. Spectra were recorded as the average of three acquisitions and corrected by subtraction of the equivalent measurements for the buffer (Figure S2).

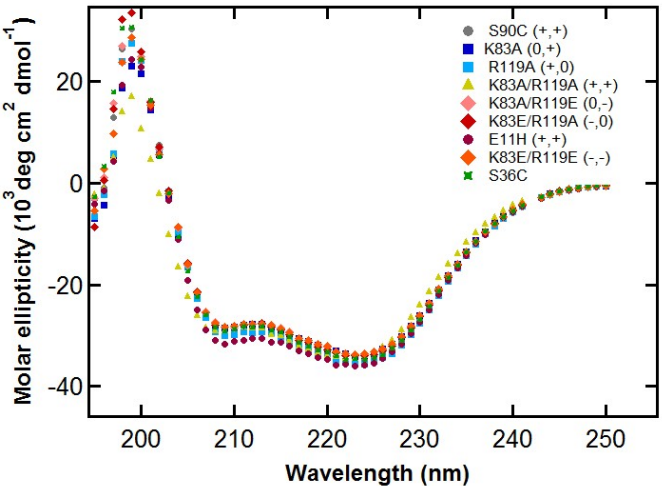

Figure S2. Circular dichroism spectra confirms the correct folded state of each lysozyme variant.

2E. Activity of lysozyme variants

The activity of each variant of lysozyme in PBS (5 μM) was measured using the EnzChek® Lysozyme Assay Kit (Invitrogen) (Fig. S3). The data show that all of the lysozyme variants were active. Under identical test conditions, each variant exhibited a different level of activity. Experiments did not attempt to compare the activities quantitatively nor identify optimum conditions for each variant.

As an additional control, the E11H variant was synthesized and attached to SWNT devices. E11H is a catalytically inactive variant[3], and it showed no activity in either the bulk assay or in the electronic single molecule measurements[1].

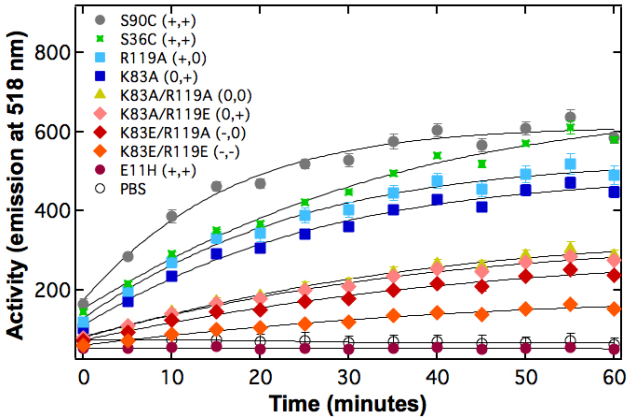

Figure S3. A fluorescence-based assay of the activity of each T4 lysozyme variant (5 μM) at 25 °C. PBS indicates a negative control with no enzyme present.

In addition, the activity of the S90C variant was measured using seven different concentrations of NaCl, buffered with 10 mM sodium phosphate at pH 7.5. As shown in Figure S4, the S90C activity was observed to be highest at 50 mM NaCl. Data points in Fig. 2b represent the average instantaneous slope at t = 0 for each concentration. Error bars in Fig. 2b represent one standard deviation from three independent measurements.

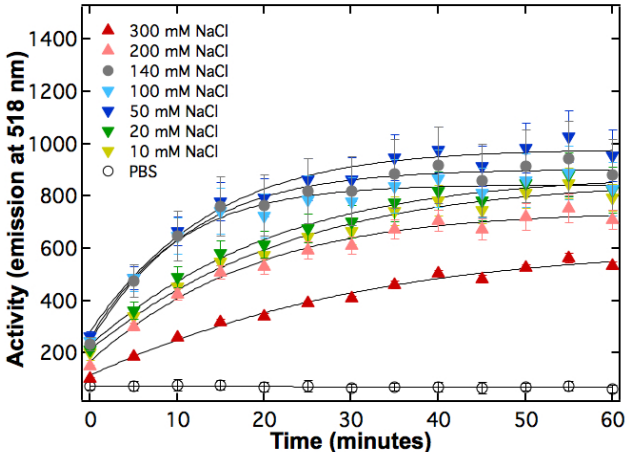

Figure S4. A fluorescence-based assay of the activity of the S90C lysozyme variant (5 μM) in solutions at the indicated NaCl concentrations. PBS indicates the negative control with no enzyme present.

3. SWNT FET Fabrication and Bioconjugation

3A. SWNT FET Fabrication

SWNTs were grown dilutely by chemical vapor deposition (CVD) directly onto 4" Si wafers using standard techniques. In our implementation, a 0.1% dilution of a saturated solution of FeMo catalyst nanoparticles in ethanol was spin-coated onto a wafer surface. The deposited catalyst clusters were oxidized at 700 C (air, 600 s), then at 940 C (520 sccm H_2 in 3000 sccm, 300 s), and then exposed to carbon feedstock (1000 sccm CH_4, 520 sccm H_2, and 3000 sccm Ar, 180 s).

After CVD, SWNT electronic devices were created using wafer-scale optical lithography. Ti electrodes with source-drain separations of 2 to 3 μm were patterned over the randomly-grown SWNTs using optical lithography with an undercut bilayer resist (S1808 over LOR-A1, MicroChem). Each device was electrically probed. To ensure that a device comprises only one SWNT, to determine the diameter of that SWNT, and to discern that the SWNT was free of particulates, each device was imaged by non-contact atomic force microscopy (AFM, NT-MDT).

After initial characterization, the device underwent a passivation step to insulate the majority of the surface including the source and drain electrodes from the protein conjugation and measurement solutions. The device was coated with an electron beam resist (A3 PMMA, MicroChem), and then patterned using electron beam lithography to expose an active SWNT window of 0.5 – 1.0 μm in length. The size of the PMMA window was also designed to maximize the probability of single-lysozyme attachments after protein conjugation.

3B. Protein Conjugation

A bi-functional linker molecule, pyrene maleimide, was used to functionalize the exposed SWNT of each device. The pyrene functionality, through pi-pi stacking, adheres strongly to sidewall of SWNT while the maleimide group allows for the formation of a stable thioether bond with the free thiol of a cysteine

sidechain in the protein. The device was submerged in a saturated solution N-(1-pyrenyl)maleimide(Sigma-Aldrich) in ethanol for 30 min without agitation. Following this, the device was rinsed with 0.1% Tween-20 (Acros Organics) in ethanol for 30 min to remove excess N-(1-pyrenyl)maleimide. After the first rinse, a second rinse was performed in a solution of 50% Tween-20 (0.1%) in ethanol and 50% phosphate buffer (20 mM Na_2HPO_4, pH 7) for 10 min with shaking to remove excess reagent. Then, the devices were rinsed under flowing de-ionized water for 5 min.

Next, a solution of a single cysteine variant of T4 lysozyme (54 μM) in phosphate buffer (20 mM Na_2HPO_4, pH 7) was prepared. At room temperature, devices were soaked in the lysozyme solution for 60 min without agitation. The devices were then washed with wash buffer (5 mM KCl, 10 mM Na_2HPO_4, 0.05% Tween-20, pH 7) for 30 min with shaking to remove unattached lysozyme. Finally, the devices were rinsed under flowing de-ionized water for 5 min. This rinsing protocol removed most but not all of the non-selectively adsorbed lysozyme from the SiO_2 surface.

To confirm protein conjugation before the electrical measurement, devices were imaged by liquid atomic force microscopy (NT-MDT) in PBS buffer. In some cases, electrical measurements were performed first, and then the devices were dried and measured in air. In both cases, all I(t) data was confirmed to be generated by a single lysozyme attachment.

4. Electrical Measurements

4A. Electrical Methods

All measurements were performed with the active portion of the device submerged in PBS buffer at pH 7.5. The potential of the electrolyte was controlled using Pt counter and pseudo-reference electrodes, and held at 0 V vs. Pt using a Keithley 2400 sourcemeter. The source-drain bias was held at 100 mV. A Keithley 428 preamplifer operating at 10^8 V/A gain and with a 40 μs rise time was used to measure the source-drain current of the device. Data was collected for at least 600 s for each measurement condition.

4B. Electronic Measurements of the S36C Variant

A S36C lysozyme variant provided an alternative attachment scheme, relocating lysozyme's hinge-bending region closer to the SWNT attachment point. Five charged residues (R14, K19, E22, E45, and K48) are proximal to a C36 site and move during hinge-bending motion, providing a means for local signal transduction.

Four SWNT devices were fabricated with S36C lysozyme and then measured with and without peptidoglycan. All four S36C devices generated two-level I(t) signals when peptidoglycan was present, and analysis determined an effective gating voltage ΔV_G = -76 ± 10 mV. This average value was twice as large as the effective gating caused by the neutral (N = 0) S90C variant.

The role of specific residues was not investigated in the S36C variant because the I(t) signal was of much poorer quality than in the S90C case. Specifically, the I(t) signals from S36C exhibited a time-varying mixture of components that was not limited to two-level switching. Two-level switching was frequently interrupted by higher frequency oscillations or noise (Fig. S5a), or multi-level fluctuations (Fig. S5b), neither of which were present in S90C data. The transient and less predictable nature of the S36C I(t) signal was poorly suited to the simple filtering used for analyzing the S90C data. The additional signal components may have been associated with motional degrees of freedom that were unique to the C36 site, but objective analysis of that possibility will require the development of new algorithms and is outside the scope of this report. In any case, signal differences between the S90C and S36C variants supports the overall conclusion that signal transduction is predominantly due to electrostatic interactions between charge residues near the attachment site and the SWNT device.

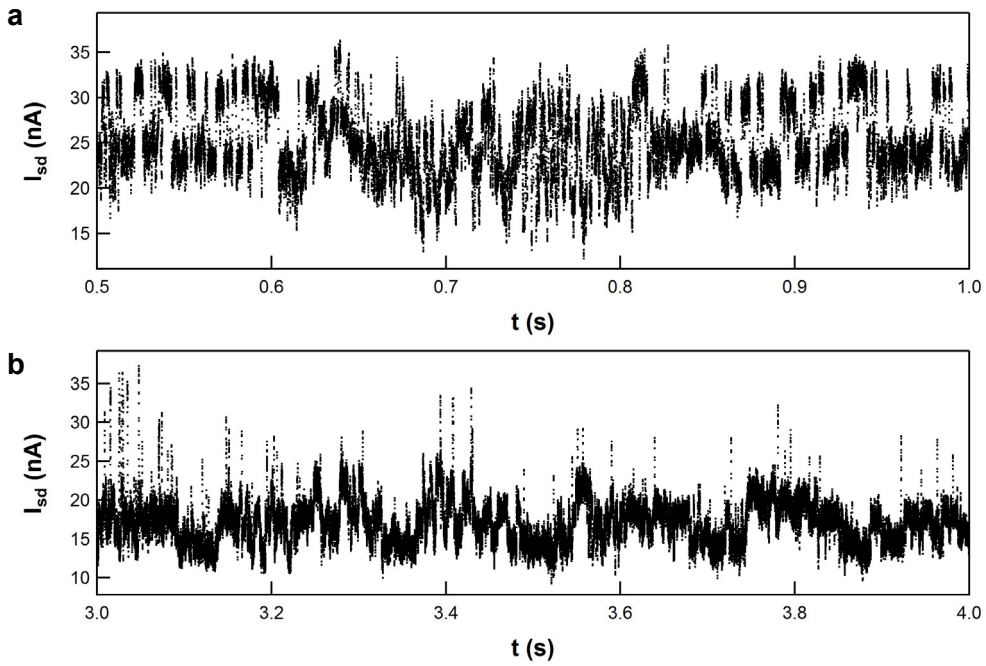

Figure S5. Examples of single molecule measurements with the S36C variant, in which simple two-level switching is accompanied by higher-frequency fluctuations (a) and/or multi-level switching (b).

4C. Electrical Noise of SWNT Devices

Devices are electrically characterized throughout the preparation and bioconjugation process. In particular, we analyze the noise and distribution of fluctuations associated with each pristine device, discarding SWNT devices unless they exhibit the 1/f noise spectra characteristic of SWNTs[4].

Furthermore, the noise characteristics of SWNT devices are typically unchanged by bioconjugation (Figure S6). Direct comparison of the spread of fluctuations $\Delta I(t)$ around a time-averaged mean cannot distinguish the addition of protein to a device. The similarity in Fig. S6c indicates that lysozyme's native variability and thermal fluctuations do not induce noise above the baseline electrical noise generated by the SWNT itself. Small changes in the DC conductance do occur, as detailed previously[1], and the precise spectral content of the noise can vary from one device to another; however, these changes do not affect the current distribution, which is the primary metric analyzed in this paper.

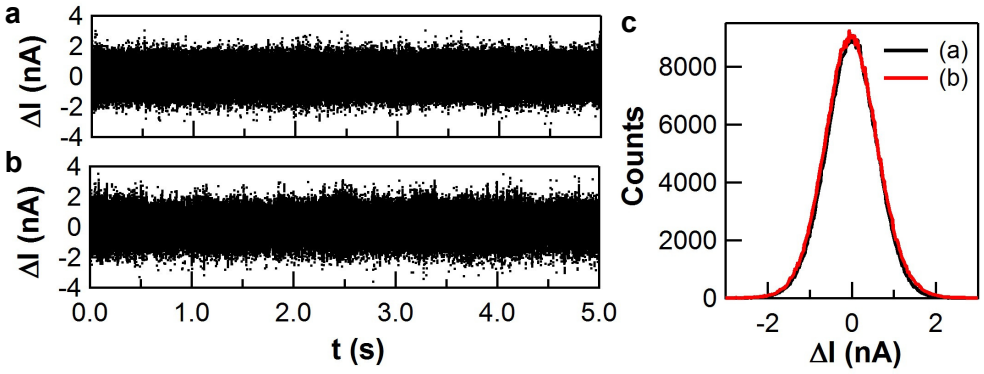

Figure S6. *I*(t) signals from a typical SWNT device (a) before and (b) after lysozyme bioconjugation. (c) Histograms of the two signal distributions are indistinguishable.

5. Analysis of Effective Gating ΔV_G in Individual S90C Devices

As described in the text, multiple electrical parameters were measured for each device. Two parameters that proved important for comparisons among devices were the size of two level fluctuations $\Delta I(t)$ and the device's intrinsic sensitivity to electrolytic gating $I(V_G)$. The relevant portion of $I(V_G)$ is the mean transconductance, or slope $\Delta I/\Delta V_G$, in the vicinity of the $V_G = 0$ operating point, as depicted graphically in Fig. 4. The quotient of the fluctuation magnitude $\Delta I(t)$ divided by the transconductance $\Delta I/\Delta V_G$ is lysozyme's effective gating ΔV_G for any particular device. The ΔV_G responses in Fig. 5 represent average values obtained in this work.

Other than these two parameters, most other electrical characterization proved inconsequential to lysozyme transduction. In particular, we observed no dependence on device-to-device variation in resistance, nor to the precise characterization of each SWNT as semiconducting or metallic. Device resistances varied widely from 0.2 MΩ to 20 MΩ, a typical range for SWNT FET research that is associated with the contact resistance to individual SWNTs [5-8]. Because all of the measurements were performed with a fixed bias voltage of 100 mV, this resistance variation caused some devices to have mean currents $\langle I(t) \rangle$ of up to 500 nA while others carried as little as 5 nA. The magnitude of lysozyme-driven, two-level fluctuations increased proportionally to this mean value $\langle I(t) \rangle$.

Figure S7 summarizes the individual responses from each of 30 different SWNT devices tested, color coded according to the particular variant of lysozyme attached. This scatter plot shows the fluctuation magnitude $\Delta I(t)$ and the transconductance $\Delta I/\Delta V_G$ of each device, normalized by $\langle I(t) \rangle$. Normalization had no effect on the computed value of ΔV_G from any individual device, but it does lead to the very effective graphical representation shown here. On normalized axes, all of the data from samples with one particular variant lie on the straight line corresponding to a singular ΔV_G value.

The graphical representation of Fig. S7 proved useful for guiding ongoing experimentation. It became clear that more precise values of ΔV_G could be obtained from line fits in Fig. S7 so long as devices covered a wide range of $\Delta I/\Delta V_G$. Initial efforts fabricating many devices with a particular variant (e.g. S90C) were replaced by a more methodical effort to select devices spanning a wide range of $\Delta I/\Delta V_G$. (e.g. K83A/R119A and K83E/R119A). Using this technique, comparably small ΔV_G error bars were achieved for each variant using as few as three or four devices in some cases.

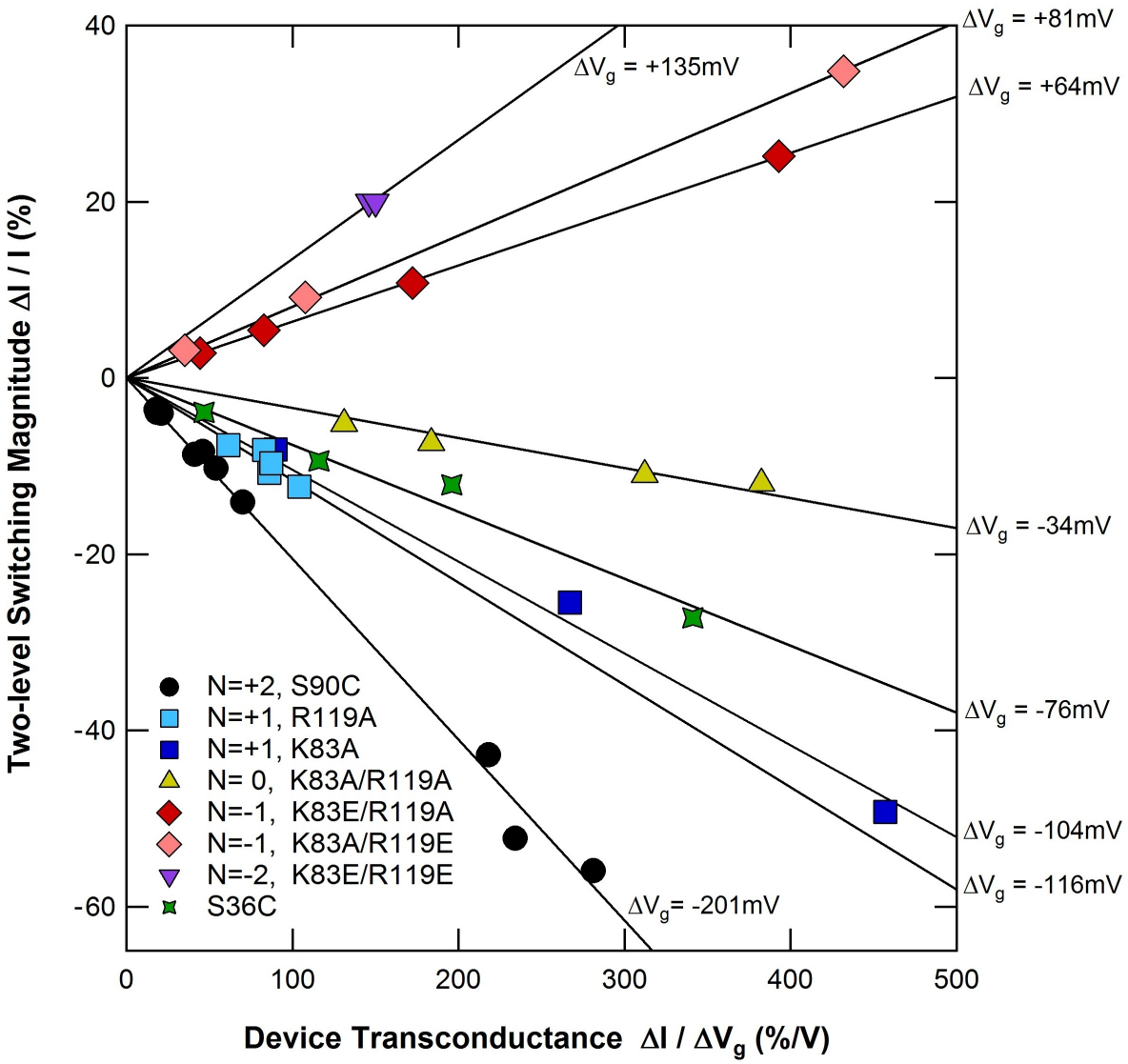

Figure S7. Compilation of switching amplitudes for all seven S90C variants and the S36C variant. Each data point represents one SWNT device functionalized with one of the possible lysozyme variants.

6. Electric Field Estimates

Vector electric fields resulting from charged sidechains at positions 83 and 119 were calculated in *Mathematica* using the three-dimensional crystal structure data for T4 lysozyme. Table S1 lists magnitudes of the key parameters and results for each variant.

According to the structural data, the sidechains at positions 83 and 119 move exactly 0.154 and 0.158 nm, respectively, away from the C90 site as the enzyme closes. Table S1 provides estimates of the corresponding movements Δr relative to the center of the pyrene ring in the pyrene-maleimide linker molecule, and directly adjacent to the SWNT. The exact pyrene-maleimide orientation is shown in Fig. 3 and, as described in the text, is one of two possible rotamers. Electric fields were next calculated for point charges at the stated distances, assuming a uniform medium with dielectric constant $\varepsilon/\varepsilon_o = 8$ and a Debye screening length $\lambda_d = 0.9$ nm accounting for the ionic concentration of the PBS buffer. The inclusion of Debye screening has a large effect, decreasing the calculated field magnitudes by 65 to 75%.

Therefore, the Debye model potentially adds significant errors to the calculation, since it does not account for the effects of surface charges, the exclusion of ions in the volume occupied by the protein, or image charges induced on the SWNT.

Table S1. Electric field magnitudes generated by point charges of interest.

	K83E/ R119E	K83A/ R119E	K83E/ R119A	K83A/ R119A	K83A	R119A	S90C
N	-2	-1	-1	0	+1	+1	+2
Q_{83}	-1	0	-1	0	0	+1	+1
$r_{83,\ open}$ (nm)*	2.33		2.33			2.33	2.33
$r_{83,\ closed}$ (nm)*	2.51		2.51			2.51	2.51
$\Delta\lvert r_{83}\rvert$ (nm)*	0.18		0.18			0.18	0.18
Q_{119}	-1	-1	0	0	+1	0	+1
$r_{119,\ open}$ (nm)*	1.90	1.90			1.90		1.90
$r_{119,\ closed}$ (nm)*	1.98	1.98			1.98		1.98
$\Delta\lvert r_{119}\rvert$ (nm)*	0.09	0.09			0.09		0.09
E_{open} (V/μm)	-26.9	-18.4	-8.9		18.4	8.9	26.9
E_{closed} (V/μm)	-22.0	-16.5	-6.6		16.5	6.6	22.0
ΔE (V/μm)	4.9	1.9	2.2	0.0	-1.9	-2.2	-4.9
ΔV_G (mV) (expt.)	135	81	64	-34	-104	-116	-205
ΔV_G+ 34 mV	169	115	98	0	-70	-82	-171

∗measured relative to the center of pyrene-maleimide.

Table S1 shows that position 83 is further from the pyrene-maleimide than position 119, but that the change $\Delta|r_{83}|$ is twice as much as $\Delta|r_{119}|$. Consequently, the two charges produce changing electric fields ΔE that are similar in magnitude. Specifically, the calculation predicts that a single charge should have a 15% greater effect when located at position 83 (e.g. R119A) than when located at position 119 (e.g. K83A). Experimentally, ΔV_G is indeed 17% higher for R119A than for K83A. However, the relative magnitudes are reversed for the variants K83A/R119E and K83E/R119A having double mutations. The text notes that the charge-symmetric portion of the response $d\Delta V_G/dN$ may be the more appropriate measure of each position's relative importance. According to that measure, the two sites are nearly identical, and the main difference in their response can be attributed to a charge-independent offset. Correctly predicting the magnitude of such offsets will require more accurate modeling of the entire protein, including its through-space screening.

References

1. Choi, Y.; Moody, I. S.; Sims, P. C.; Hunt, S. R.; Corso, B. L.; Weiss, G. A.; Collins, P. G. *Science* **2012,** 335, 319-324.
2. Choi, Y.; Moody, I. S.; Sims, P. C.; Hunt, S. R.; Corso, B. L.; Seitz, D. E.; Blaszcazk, L. C.; Collins, P. G.; Weiss, G. A. *J. Am. Chem. Soc.* **2012,** 134, 2032-2035.
3. Shiu, Y.-J.; Jeng, U. S.; Huang, Y.-S.; Lai, Y.-H.; Lu, H.-F.; Liang, C.-T.; Hso, I. J.; Su, C.-H.; Su, C.; Chao, I.; Su, A.-C.; Lin, S.-H. *Biophysical Journal* **2008,** 94, 4828-4836.

4. Collins, P. G.; Fuhrer, M. S.; Zettl, A. *Appl. Phys. Lett.* **2000,** 76, 894-896.
5. Kim, W.; Javey, A.; Tu, R.; Cao, J.; Wang, Q.; Dai, H. J. *Appl. Phys. Lett.* **2005,** 87.
6. Mann, D.; Javey, A.; Kong, J.; Wang, Q.; Dai, H. J. *Nano Lett.* **2003,** 3, 1541-1544.
7. Chen, Z. H.; Appenzeller, J.; Knoch, J.; Lin, Y. M.; Avouris, P. *Nano Lett.* **2005,** 5, 1497-1502.
8. Tseng, Y. C.; Phoa, K.; Carlton, D.; Bokor, J. *Nano Lett.* **2006,** 6, 1364-1368.